Article in Bone · January 2017 - DOI: 10.1016/j.bone.2017.01.016

µCT-based trabecular anisotropy can be reproducibly computed from HR-pQCT scans using the triangulated bone surface

Hadi S. Hosseini [a*], Ghislain Maquer [a*] and Philippe K. Zysset [a]

[a] *Institute for Surgical Technology and Biomechanics, University of Bern, Stauffacherstr. 78, CH-3014 Bern, Switzerland*

[*] *Hadi Hosseini and Ghislain Maquer contributed equally to this work and request acknowledgment of double first authorship.*

Corresponding author: Ghislain Maquer (ghislain.maquer@istb.unibe.ch)

Other authors: hadi.seyedhosseini@gmail.com, philippe.zysset@istb.unibe.ch

Abstract word count: 244

Total word count: 3727

Attachments: 4 figures and 2 tables

Article in Bone · January 2017 - DOI: 10.1016/j.bone.2017.01.016

Highlights

- A new method for evaluating the fabric tensor from triangulated bone surfaces was introduced: the mean surface length (MSL)
- 24 human radii were scanned via low and high resolution HR-pQCT protocols repeated three times and μCT
- The performance and reproducibility of MSL, MIL, GST and SCANCO's TRI were compared using 182 regions of interest
- MSL derived from HR-pQCT was the best surrogate for the gold standard MIL on μCT
- MSL was more reproducible than MIL for capturing the fabric tensor from HR-pQCT

Article in Bone · January 2017 - DOI: 10.1016/j.bone.2017.01.016

Abstract

The trabecular structure can be assessed at the wrist or tibia via high-resolution peripheral quantitative computed tomography (HR-pQCT). Yet on this modality, the performance of the existing methods, evaluating trabecular anisotropy is usually overlooked, especially in terms of reproducibility. We thus proposed to compare the TRI routine used by SCANCO Medical AG (Brüttisellen, Switzerland), the classical mean intercept length (MIL), and the grey-level structure tensor (GST) to the mean surface length (MSL), a new method for evaluating a second-order fabric tensor based on the triangulation of the bone surface. The distal radius of 24 fresh-frozen human forearms was scanned three times via HR-pQCT protocols (61µm, 82µm nominal voxel size), dissected, and imaged via micro computed tomography (µCT) at 16µm nominal voxel size. After registering the scans, we compared for each resolution the fabric tensors, determined by the mentioned techniques for 182 trabecular regions of interest. We then evaluated the reproducibility of the fabric information measured by HR-pQCT via precision errors. On µCT, TRI and GST were respectively the best and worst surrogates for $MIL_{\mu CT}$ (MIL computed on µCT) in terms of eigenvalues and main direction of anisotropy. On HR-pQCT, however, MSL provided the best approximation of $MIL_{\mu CT}$. Surprisingly, surface-based approaches (TRI, MSL) also proved to be more precise than both MIL and GST. Our findings confirm that MSL can reproducibly estimate $MIL_{\mu CT}$, the current gold standard. MSL thus enables the direct mapping of the fabric-dependent material properties required in homogenised HR-pQCT-based finite element models.

Keywords: trabecular bone, anisotropy, fabric tensor, reproducibility, high-resolution peripheral quantitative computed tomography, micro computed tomography.

Article in Bone · January 2017 - DOI: 10.1016/j.bone.2017.01.016

1. Introduction

Millions of fractures are attributed to osteoporosis, a condition inducing bone loss and impairing the trabecular bone structure (Johnell and Kanis, 2006). The World Health Organisation recommends the evaluation of bone density at the hip and spine by DXA (dual X-ray absorptiometry) to detect the disease. Yet, there is currently no mass screening (Richy et al. 2004) and many fracture patients were not considered at risk according to DXA-based diagnoses (Langsetmo et al. 2009). Osteoporosis is under-diagnosed and often discovered too late: when fracture occurs (Gasser et al. 2005).

Wrist fractures often happen earlier in life than more deleterious incidents at the hip or spine (Cuddihy et al. 1999) and can thus be seen as precursory signs. Following the introduction of high-resolution peripheral quantitative computed tomography (HR-pQCT), a plethora of structural indices, initially developed for micro CT (µCT) of bone biopsies (Odgaard 1997), was adapted to the new modality. The hope was to refine the fracture risk assessment thanks to the *in vivo* characterization of the trabecular architecture of the distal radius (Boutroy et al. 2005).

To various extent, these structural indices predict the mechanics of cancellous bone (MacNeil and Boyd 2007a, Liu et al. 2010), but they are also highly related with one another (Hildebrand et al. 1999, Liu et al. 2010). In this context, bone volume over total volume (BV/TV) and the fabric tensor, a second-rank tensor describing the trabecular anisotropy (Cowin 1985), stand out. Independent from each other, they predict 97% of the elastic and yield properties of trabecular bone with fabric explaining 10 to 20% of the variation (Maquer et al. 2015, Musy et al. 2017). BV/TV and fabric constitute a basis for homogenised HR-pQCT-based finite element (hFE) models, computing bone strength faster than micro finite element (µFE) standards (Varga et al. 2011, Hosseini et al. 2017).

A multitude of approaches can evaluate the trabecular anisotropy via fabric tensors (Moreno et

al. 2014). Among those, the mean intercept length (MIL) is the gold standard for deriving fabric tensors (Whitehouse 1974, Harrigan and Mann 1984). Used for decades, MIL is the method of choice for predicting the mechanical behaviour of the trabecular structure (Zysset 2003). Following a trend initiated for other indices (Müller et al. 1994, 1998), an alternative was proposed to evaluate the fabric anisotropy from the triangulation of the bone surface: TRI (Laib et al. 2000). Most users may not be aware of it, but the TRI method is used by default in the evaluation protocol of the XtremeCT (XtremeCTII, User's Guide, Revision 2.6), the only device currently able to conduct *in vivo* HR-pQCT scans (SCANCO Medical AG, Brüttisellen, Switzerland). Both methods have shortcomings: MIL relies on segmented CT images with sufficiently small voxel sizes (82 to 90-µm nominal voxel size maximum) while TRI requires an extra processing step relative to the surface triangulation. The grey-level structure tensor (GST) was thus proposed to provide fabric information directly from the intensity values of CT images (Rao and Schnunck 1991, Tabor and Rokita 2007).

Structural indices, obtained from HR-pQCT reconstructions, are regularly compared to their gold-standard µCT measurements (MacNeil and Boyd 2007b, Sode et al. 2008, Krause et al. 2014, Zhou et al. 2016) and their short-term reproducibility has been assessed in several occasions (Müller et al. 1996, Boutroy et al. 2005, Krause et al. 2014). Despite its importance in bone mechanics (Cowin 1985, Odgaard et al. 1997), anisotropy is either overlooked or reduced to the simplistic degree of anisotropy (DA) in those studies. Besides, even if TRI was designed to reproducibly mimic MIL by avoiding the use of test lines (Laib et al. 2000), its superior reproducibility has never demonstrated.

In this context, the aim of this work is two-fold: first, we introduce a simpler method for measuring the trabecular anisotropy from triangulated bone surfaces: the mean surface length (MSL). Second, we compare the fabric information and the reproducibility of MSL, TRI, MIL, and GST using trabecular regions of the distal radius scanned via µCT and HR-pQCT devices.

Article in Bone · January 2017 - DOI: 10.1016/j.bone.2017.01.016

2. Materials and methods

2.1. Presentation of the mean surface length

TRI (Laib et al. 2000) and the mean surface length (MSL) rest on the triangulation of the bone surface based on the marching cubes algorithm (Lorensen and Cline 1987) (Fig. 1). TRI relies on the normal unit vectors of each triangle ($\|\mathbf{n^i}\| = 1$) to generate a MIL-like orientation distribution on which an ellipsoid is fitted to produce a second-order tensor. The MSL fabric tensor, on the other hand, is directly based on the dyadic product of the normal unit vectors (He and Curnier 1995) and does not necessitate an ellipsoid fit. Those dyadic products are weighted by the area of the corresponding triangles (A_i) and summed up until all the triangles composing the bone surface (i_{max}) are accounted for:

$$\mathbf{A} = \sum_{i=1}^{i_{max}} A_i(\mathbf{n}_i \otimes \mathbf{n}_i) \quad (1)$$

By construction, **A** is an invertible symmetric positive-definite second-order tensor. Yet, the eigenvector related to its smallest eigenvalue corresponds to the main material orientation, which is counter-intuitive, and its eigenvalues have the unit of a surface. **A** is thus inverted and multiplied by BV, the total volume of the segmented microstructure (bone volume). The resulting tensor is scaled by a factor 2 to ensure that the mean length of the material is equivalent to the one measured by Cowin's fabric tensor in the case of a hexahedron (Cowin 1986):

$$\widetilde{\mathbf{H}} = 2\ BV\ \mathbf{A}^{-1} \quad (2)$$

$\widetilde{\mathbf{H}}$ is finally normalized into a dimensionless second-order tensor (Zysset and Curnier 1995):

$$\mathbf{MSL} = \frac{3\widetilde{\mathbf{H}}}{\mathrm{trace}(\widetilde{\mathbf{H}})} \quad (3)$$

Its spectral decomposition gives $\mathbf{MSL} = \sum_{i=1}^{3} m_i(\mathbf{m_i} \otimes \mathbf{m_i})$, with $m_3 \geq m_2 \geq m_1 > 0$ being the eigenvalues and $\mathbf{m_3}$, $\mathbf{m_2}$, $\mathbf{m_1}$ being the corresponding eigenvectors of the **MSL** tensor. MSL was implemented in Fortran 95 with .stl files as input. All fabric tensors presented in this work

were normalized according to eq. 3.

For verification, MSL, MIL and GST were compared on regular structures (Fig. 2). Following Harrigan and Mann (1984), the actual MIL (exact MIL before ellipsoidal fit) and its ellipsoidal approximation were calculated analytically (Mathematica 10.4, Wolfram, USA). The structures were voxelized into binary images (10µm voxel size) (Amira 6, FEI, USA) from which GST fabric tensors were computed (Medtool 3.9, www.dr-pahr.at) (Rao and Schnunck 1991, Tabor and Rokita 2007). Finally, triangular meshes were produced from the images' isosurface via the marching cubes algorithm (Lorensen and Cline 1987) available in Paraview (4.3, Kitware, USA) and the MSL fabric tensors were evaluated. The tensors' eigenvalues, eigenvectors and degree of anisotropy (DA $= m_3/m_1$) were compared.

2.2. Preparation of the trabecular samples

After ethical approval, we obtained 24 fresh-frozen forearms from the Medical University of Vienna. The donors (7 males, 5 females, 77 ± 9 years old [65-92]) had dedicated their body to research by informed consent. The forearms were thawed at room temperature a day before HR-pQCT measurements (XtremeCTII, SCANCO Medical AG, Brüttisellen, Switzerland). Low resolution **LR** (82µm, 68kV, 1460µA, 36ms) and high resolution **HR** (61µm, 68kV, 1460µA, 43ms) scanning protocols corresponding to the XtremeCT and XtremeCTII (the former and new scanner generations) acquisitions were used. The distal section of the radius of each forearm was scanned and repositioned three times with LR and HR protocols, the focus being a 20mm-thick section located 9mm below the distal subchondral plate (Fig. 1). Three trained operators performed the scans (Hadi Hosseini, Andreas Dünki, and Jonas Fabech). The radii were then dissected from the forearms, the scanned sections cut off using a diamond-coated band saw (Exakt 30, Exakt Technologies, USA) and the bone marrow removed. The cleaned bone sections were then placed in a radio-transparent container filled with saline water. After vacuuming the air bubbles, the sections were scanned using µCT100 (SCANCO Medical

AG, Brüttisellen, Switzerland - 16.4µm, 70kV, 200µA, 300s). The HR-pQCT and µCT reconstructions were brought into one coordinate system using the 6D (three translations and three rotations) rigid registration algorithm (MacNeil and Boyd 2008) of the Elastix software (Klein et al. 2010). Finally, cubic samples (6mm edge length) were cropped virtually from the trabecular compartment (Fig. 1) to cover a wide range of BV/TV (Table 1). A cohort of 182 cubes scanned at least once at each resolution (µCT, HR, LR) was produced, 56 of which had been imaged three times with the HR and LR protocols.

2.3. Computation of the fabric tensors

First, each cube was imported back to the XtremeCT to be pre-processed via SCANCO's IPL (image processing language) according to the manufacturer's procedures. A 3D Gaussian filter ($\sigma = 0.8$ and support = 1) was used on the HR and µCT cubes to reduce noise, while a 3D Laplace-Hamming filter was applied to the LR cubes for the same reason (Laib and Ruegsegger, 1999). All specimens were finally segmented with a fixed threshold (320 mgHA.cm^{-3}).

All fabric tensors were calculated for a 6 mm diameter spherical region of interest located in the centre of each cube (Fig. 1). Only the TRI analyses were conducted in IPL. We exported the grey-level (before and after Gaussian filter) and the segmented cubes to perform the calculation of the other fabric tensors via Medtool 3.9 (www.dr-pahr.at) or our own code in case of MSL. The GST fabric tensors were computed for all grey-level datasets µCT, HR, LR, HR Gauss-filtered and LR Gauss-filtered. The MIL fabric tensors were evaluated from the segmented dataset via 512 directions for the test lines. It should be noted that all MIL values computed for trabecular bone cubes derive from an ellipsoidal fit. The MSL fabric tensors were measured from triangular meshes generated by Paraview (4.3, Kitware, USA) from the segmented cubes as described in section 2.1. It is also worth mentioning that the meshes went through a topology-preserving decimation (target reduction: 90%, feature angle: 15°) to speed-up the MSL computation. Bone volume over total volume (BV/TV) and degree of anisotropy

(DA), attributed to each fabric tensor, were also computed for completeness (Table 1). In practice, a python code was implemented as an interface between Paraview and the Fortran implementation of MSL. It takes a segmented image as input (.mhd + .raw) and outputs the corresponding triangulated surface (.stl) and the MSL analysis (.txt). These codes and an image example are provided as supplementary material.

2.4. Resolution-dependence and reproducibility of the fabric tensors

The impact of image resolution on the fabric tensors was assessed against a single reference $\mathbf{MIL_{\mu CT}}$, the MIL fabric tensor obtained from µCT resolution. This choice was motivated by the importance of MIL in the literature. First, there exists much evidence showing that MIL can be used for predicting the mechanical properties of trabecular bone (Cowin 1985, Cowin 1986, Maquer et al. 2015, Musy et al. 2017). Second, virtually every new measure has been compared to MIL on µCT: VO, SVD, SLD (Odgaard et al. 1997), SSOD (Varga and Zysset 2009a), GMIL (Moreno et al. 2014), GST (Tabor 2012, Nazemi et al. 2016) and so on. Even TRI has been designed to replicate MIL on µCT, but with better reproducibility (Laib et al. 2000).

As a strong relationship ties fabric tensors obtained from different approaches ($\widehat{\mathbf{M}}$), a power law (Larsson et al. 2014) was used to evaluate the agreement of their eigenvalues ($\widehat{m}_i$) against those of $\mathbf{MIL_{\mu CT}}$ (m_i) while preserving their normalization (eq. 3):

$$m_i = \frac{3\widehat{m}_i^k}{\sum_{\mathrm{j}=1}^{3} \widehat{m}_j^k}, \mathrm{i} = 1,3 \tag{4}$$

Exponent *k* served as the first comparison point. Independently of the goodness of fit (R^2) and root-mean-square errors (rmse), $k>1$ implies that m_i are more spread than $\widehat{m}_i$, while $k<1$ means that m_i are more contracted, $k=1$ being a perfect match. Another aspect that was accounted for was the orientation of the tensors relative to $\mathbf{MIL_{\mu CT}}$. Our second comparison point, θ, was thus defined as the absolute angular difference between the main eigenvector of $\widehat{\mathbf{M}}$ ($\widehat{\mathbf{m}}_\mathbf{3}$) and $\mathbf{MIL_{\mu CT}}$ ($\mathbf{m_3}$). The two aspects were also used to evaluate the methods' short-term

reproducibility (Glüer et al 1995). Precision errors were computed for the HR and LR cubes as the coefficient of variation of the tensors' main eigenvalue ($PE_{eigenvalue}$) and main eigenvector ($PE_{eigenvector}$). The short-term reproducibility of the µCT cubes was not evaluated, for they were scanned only once.

3. Results

3.1. Comparison of the fabric tensors of regular structures

MIL, GST and MSL established that the structures indeed featured transverse isotropy with a main eigenvector oriented along direction 3 (Fig. 2). Compared to the actual MIL, the ellipsoidal fit emphasized the main eigenvalue (m_3) to the detriment of its transverse eigenvalues (m_1, m_2), resulting in a larger DA. The contrary holds for GST that yielded a much lower DA. For the hexahedron, MSL's fabric was close to the actual MIL. For the two other structures (full and truncated octahedra), MSL's fabric was equivalent to MIL's ellipsoidal fit.

3.2. Comparison of the fabric tensors from µCT images

On µCT, TRI and GST were respectively the best and worst surrogates for MIL in terms of eigenvalues and main orientation (Fig. 3). Although the power fit (eq. 4) was good for all methods (R^2>0.96), GST's eigenvalues were contracted compared to those of $\mathbf{MIL_{\mu CT}}$ (k = 0.4), MSL's were spread (k = 1.38), and only TRI offered a match (k ~ 1). The angular deviation between the main eigenvector of those fabric tensors and $\mathbf{MIL_{\mu CT}}$ was low in case of GST and MSL (θ~1°), but even lower with TRI (θ~0.5°). The maximal deviation from $\mathbf{MIL_{\mu CT}}$ was observed with GST and exceeded 9°, instead of 5° for TRI and MSL.

3.3. Effect of image resolution on the fabric tensors

Contraction of the eigenvalues (k=0.81) and deviation from $\mathbf{MIL_{\mu CT}}$'s main direction by 2.54° were induced when MIL was computed on the HR cubes (Table 2). Little changes were observed after further coarsening (LR). GST, however, was altered after each coarsening. Its k

exponent improved only to reach 0.59 on the LR scans and θ doubled from 1.18° to 2.51° between the μCT and LR resolutions. The Gauss filter improved the correspondence between the eigenvalues of GST and $\mathbf{MIL_{\mu CT}}$ (k up to 0.64). Despite being computed from surface meshes, HR-pQCT-based TRI and MIL were similarly influenced by the change in nominal voxel size ($0.75<k<0.79$, $2.22°<\theta<2.32°$). On both HR-pQCT protocols, MSL provided the best approximation of $\mathbf{MIL_{\mu CT}}$ in terms of eigenvalues and main orientation (k~1 and θ~2°).

3.4. Reproducibility of the HR-pQCT-based fabric tensors

The reproducibility was assessed for both HR-pQCT protocols (Fig. 4). In general, the reproducibility was higher for the main eigenvalue (m_3) than for the main eigenvector ($\mathbf{m_3}$) and higher with HR protocol than for LR. In terms of m_3, precision errors were low for all methods. TRI ($PE_{eigenvalue}<0.7\%$) was the most reproducible approach, GST ($PE_{eigenvalue}<1.5\%$) the least. The precision of $\mathbf{m_3}$ showed more disparity, with MIL being less reproducible ($PE_{eigenvector}$ up to 5%) than the other techniques ($PE_{eigenvector}<3.3\%$). Finally, the application of the Gauss filter on the grey-level HR-pQCT scans improved the precision of the GST fabric tensor by up to 0.5%.

4. Discussion

There are numerous ways for quantifying the trabecular anisotropy, but surprisingly, little is known about their accuracy and precision on HR-pQCT data, especially for the HR protocol of the XtremeCTII. We thus proposed to compare the fabric tensors provided by surface-based methods, SCANCO's TRI and our new mean surface length (MSL), to well established methods such as mean intercept length (MIL) and grey-level structure tensor (GST) on HR-pQCT and μCT scans of the distal radius.

The MIL-based fabric depends on the bone segmentation, particularly for lower resolution data such as HR-pQCT, where thin structures are easily missed with the wrong threshold (Varga and Zysset 2009b). In this work, we mimicked SCANCO's image pre-processing, but MIL

remained influenced by the image resolution. The use of random test lines is also known to contribute to the reproducibility error of MIL (Simmons and Hipp 1997) and MIL is indeed the least precise of the tested techniques. Grey-level methods were developed to avoid these two issues. Indeed, the main direction of anisotropy computed via GST on HR-pQCT coincides with $\mathbf{MIL_{\mu CT}}$'s main orientation better than MIL's. GST is also more reproducible, especially if a Gaussian filter is used to reduce the noise in the raw images. However, GST underestimates greatly the degree of anisotropy of regular and trabecular structures, even if the Gauss filter also improves the correspondence with MIL as suggested by Tabor (2012).

TRI was introduced as an equivalent to MIL on µCT images and was also designed to be more reproducible (Laib et al. 2000). Both aspects are supported by our results. The improved precision may be surprising because the surface triangulation could appear as an additional source of error. Yet, if every triangle of the surface is accounted for - and there is no mention of random sampling in Laib et al. (2000) - the extra variation is low. The size and amount of triangles, however, scales with the voxel size (Lorensen and Cline 1987), explaining TRI's sensitivity to the image resolution.

MSL also rests on a triangle mesh, but differs from TRI on several points. First, the marching cubes algorithm was used to generate the surface meshes, but the implementations used in IPL (used for TRI) and Paraview (used for MSL) may differ. Second, unlike TRI, our calculation of MSL was based on decimated meshes to speed-up its computation. The computation time of MSL and TRI depends on the amount of triangles needed to describe the bone surface. TRI is only available in IPL and was evaluated on the powerful workstation provided along the scanner. MSL, however, was computed on a desktop machine with one CPU, hence the decimation. The target of the decimation was to remove up to 90% of the triangles to ensure the highest speed gain (about 20% faster), but in practice, the topology-preserving decimation stops as soon as the topology is being compromised. The norm errors induced by the decimation

were below 0.05% on both µCT and HR-pQCT cubes. Finally, MSL does not attempt to mimic MIL as TRI does. Without ellipsoid fit, MSL seems more sensitive to the shape of the structure and reflects the three main fabric directions better than MIL almost without deviating from **$MIL_{\mu CT}$**'s main direction. Still, MSL is affected by the resolution and its eigenvalues calculated from HR-pQCT coincide better with the ones from **$MIL_{\mu CT}$** than other approaches. The interpretation for this unexpected feature is that the HR-pQCT resolution degrades MSL as much as the ellipsoid fit degrades **$MIL_{\mu CT}$**.

The relevance of this work goes beyond the sole comparison of fabric measurements. Although a fracture is triggered by random events (e.g. fall), it also depends largely on the load bearing capacity of the trabecular structure. Knowledge of bone strength can actually improve the fracture predictions at the wrist (Boutroy et al. 2008) and other sites at risk (Nishiyama et al. 2013). That is where the fabric tensor comes into play. Combined with BV/TV, the fabric tensor offers better predictions of the mechanical properties of trabecular structure than other morphological indices (Maquer et al. 2015, Musy et al. 2017). Consequently, HR-pQCT-based hFE models rely on BV/TV and fabric-dependent material properties to compute bone strength quicker than µFE (Varga et al. 2011). These material properties are often derived from µCT using MIL (Gross et al. 2013, Panyasantisuk et al. 2015, Latypova et al. 2016) to avoid the hassle of determining new material parameters for each method, resolution, anatomical site, acquisition protocol, and reconstruction kernel (Nazemi et al. 2016). Underestimating anisotropy would result in the poor description of the orthogonal mechanical properties of the trabecular region. In this case, the HR-pQCT-based MIL fabric has to be scaled to compensate for the lower resolution (Varga and Zysset 2009b). Yet, if a relationship between eigenvalues is missing, MSL is a good option as it does not deviate much from **$MIL_{\mu CT}$**. MSL is as reproducible as TRI, but unlike SCANCO's proprietary method, its implementation is open source (our code is provided as supplementary material). Finally, MSL has already been used

in hFE models predicting the stiffness and failure loads of human distal radii (Hosseini et al. 2017).

To our knowledge, this is the first time that detailed fabric evaluations are conducted on data from the new HR-pQCT scanner generation (XtremeCTII). Three CT modalities were really used, instead of downscaling µCT images as often done (Nazemi et al. 2016). Our study is also the only publicly available document evaluating SCANCO's routine TRI against other techniques. We also looked at the precision error of the HR-pQCT-based fabric tensor, including its main orientation, while authors restrict their effort to the degree of anisotropy (Müller et al. 1996, Boutroy et al. 2005, MacNeil and Boyd 2007b, Sode et al. 2008, Krause et al. 2014, Zhou et al. 2016). Besides, although TRI is the standard method, MIL is also available in IPL (SCANCO's image processing language), but authors do not report which one they used. Our findings show that using one or the other method on HR-pQCT data has an impact on the absolute measure of DA. Finally, unfixed anatomical specimens of human forearms were used to mimic the *in vivo* conditions and 20 mm sections were scanned instead of the standard 10 mm to cover the entire region at risk of Colles' fracture (Eastell et al. 1996). The cubes extracted from such larger regions featured a wide variety of morphologies (wide range of BV/TV and DA displayed in Table 1) and we can reasonably speculate that our results would hold at the tibia, the second site for *in vivo* HR-pQCT imaging.

In spite of obvious strengths, our work entails limitations that must be discussed. For instance, the fabric tensors involved in this study were all second-order as the trabecular structure was assumed orthotropic (Zysset and Curnier 1995). Fourth-order fabric tensors would be an alternative in regions where the orthotropy assumption is not fulfilled (Moreno et al. 2015). Then, although all eigenvalues were involved in our analyses, the study of the fabric's orientations focused on the main direction of anisotropy ($\mathbf{m}_3$). Finally, we did not consider the motion artefacts occurring during *in vivo* scans, but accounted for the operator variability via

three operators. The influence of both aspects can be minimized (Pauchard et al. 2012, Bonaretti et al. 2016).

Despite the additional interpolation relative to the surface triangulation, MSL provides reproducible estimates of the μCT-based MIL fabric tensor, the current gold standard, from HR-pQCT reconstructions. Thanks to MSL, morphology-dependent material properties, originally established using MIL and μCT scans, can be used in homogenised HR-pQCT-based finite element models directly. TRI, SCANCO's standard method for measuring trabecular anisotropy, is also highly reliable, but its implementation is not publicly available.

Article in Bone · January 2017 - DOI: 10.1016/j.bone.2017.01.016

Acknowledgments

The authors acknowledge Michael Pretterklieber (Department of Applied Anatomy, Medical University of Vienna, Austria) for organising the human material and Martin Stauber (SCANCO Medical AG, Brüttisellen, Switzerland) for conducting the TRI analyses. Thanks to Andreas Dünki and Jonas Fabech (Institute for Surgical Technology and Biomechanics, University of Bern, Switzerland) for helping with the HR-pQCT scans. This research was made possible through funding from the Swiss Commission for Technology and Innovation CTI (14311.1 PFLS-LS) and the Gebert Rüf Foundation (GRS-079/14).

Article in Bone · January 2017 - DOI: 10.1016/j.bone.2017.01.016

References

[1] Bonaretti, S., Vilayphiou, N., Chan, C.M. et al. Operator variability in scan positioning is a major component of HR-pQCT precision error and is reduced by standardized training. Osteoporos Int (2016). doi:10.1007/s00198-016-3705-5

[2] Boutroy, S., Bouxsein, M. L., Munoz, F., & Delmas, P. D. (2005). In vivo assessment of trabecular bone microarchitecture by high-resolution peripheral quantitative computed tomography. The Journal of Clinical Endocrinology & Metabolism, 90(12), 6508-6515.

[3] Boutroy, S., Van Rietbergen, B., Sornay-Rendu, E., Munoz, F., Bouxsein, M. L., & Delmas, P. D. (2008). Finite element analysis based on in vivo HR-pQCT images of the distal radius is associated with wrist fracture in postmenopausal women. Journal of Bone and Mineral Research, 23(3), 392-399.

[4] Bouxsein, M. L., Boyd, S. K., Christiansen, B. A., Guldberg, R. E., Jepsen, K. J., & Müller, R. (2010). Guidelines for assessment of bone microstructure in rodents using micro–computed tomography. Journal of bone and mineral research, 25(7), 1468-1486.

[5] Cowin, S. C. (1985). The relationship between the elasticity tensor and the fabric tensor. Mechanics of Materials, 4(2), 137-147.

[6] Cowin, S.C., 1986. Wolff's law of trabecular architecture at remodeling equilibrium. Journal of biomechanical engineering 108, 83–88.

[7] Cuddihy MT, Gabriel SE, Crowson CS, O'Fallon WM, Melton LJ. Forearm fractures as predictors of subsequent osteoporotic fractures. Osteoporos Int 1999;9:469–75.

[8] Eastell, R. (1996). Forearm fracture. Bone, 18(3), S203-S207.

[9] Gasser, K. M., Mueller, C., Zwahlen, M., Kaufmann, M., Fuchs, G., Perrelet, R., ... & Lippuner, K. (2005). Osteoporosis case finding in the general practice: phalangeal radiographic absorptiometry with and without risk factors for osteoporosis to select postmenopausal women eligible for lumbar spine and hip densitometry. Osteoporosis international, 16(11), 1353-1362.

[10] Glüer, C.C., Blake, G., Lu, Y., Blunt, B.A., Jergas, M., Genant, H.K., 1995. Accurate assessment of precision errors: How to measure the reproducibility of bone densitometry techniques. Osteoporos. Int. 5, 262–270

[11] Gross, T., Pahr, D. H., & Zysset, P. K. (2013). Morphology–elasticity relationships using decreasing fabric information of human trabecular bone from three major anatomical locations. Biomechanics and modeling in mechanobiology, 12(4), 793-800.

[12] Harrigan, T. P., & Mann, R. W. (1984). Characterization of microstructural anisotropy in orthotropic materials using a second rank tensor. Journal of Materials Science, 19(3), 761-767.

[13] He, Q.C., Curnier, A., 1995. A more fundamental approach to damaged elastic stress-strain relations. International Journal of Solids and Structures 32, 1433–1457.

[14] Hildebrand, T., Laib, A., Müller, R., Dequeker, J., Rüegsegger, P., 1999. Direct three-dimensional morphometric analysis of human cancellous bone: microstructural data from spine, femur, iliac crest, and calcaneus. J. Bone Miner. Res. 14(7), 1167-1174.

[15] Hosseini H.S. , Dünki A. , Fabech J. , Stauber M. , Vilayphiou N. , Pahr D. , Pretterklieber M., Wandel J., van Rietbergen B. , Zysset P.K. 2017. Fast estimation of Colles' fracture load of the distal section of the radius by homogenized finite element analysis based on HR-pQCT. Bone. doi: 10.1016/j.bone.2017.01.003

[16] Johnell, O., & Kanis, J. A. (2006). An estimate of the worldwide prevalence and disability associated with osteoporotic fractures. Osteoporosis international, 17(12), 1726-1733.

[17] Klein, S., Staring, M., Murphy, K., Viergever, M., Pluim, J., 2010. Elastix: A Toolbox for Intensity-Based Medical Image Registration. IEEE Transactions on Medical Imaging 29, 196–205.

[18] Krause, M., Museyko, O., Breer, S., Wulff, B., Duckstein, C., Vettorazzi, E., ... & Amling, M. (2014). Accuracy of trabecular structure by HR-pQCT compared to gold standard μCT in the radius and tibia of patients with osteoporosis and long-term bisphosphonate therapy. Osteoporosis International, 25(5), 1595-1606.

[19] Langsetmo, L., Goltzman, D., Kovacs, C. S., Adachi, J. D., Hanley, D. A., Kreiger, N., ... & Jamal, S. A. (2009). Repeat low-trauma fractures occur frequently among men and women who have osteopenic BMD. Journal of Bone and Mineral Research, 24(9), 1515-1522.

[20] Laib, A., Ruegsegger, P., 1999. Comparison of structure extraction methods for in vivo trabecular bone measurements. Comput. Med. Imaging Graph. 23, 69–74.

[21] Laib, A., Barou, O., Vico, L., Lafage-Proust, M. H., Alexandre, C., & Rügsegger, P. (2000). 3D micro-computed tomography of trabecular and cortical bone architecture with application to a rat model of immobilisation osteoporosis. Medical and Biological Engineering and Computing, 38(3), 326-332.

[22] Larsson, D., Luisier, B., Kersh, M. E., Dall'Ara, E., Zysset, P. K., Pandy, M. G., & Pahr, D. H. (2014). Assessment of transverse isotropy in clinical-level CT images of trabecular bone using the gradient structure tensor. Annals of biomedical engineering, 42(5), 950-959.

[23] Latypova A, Maquer A, Elankumaran K, Pahr D, Zysset P, Pioletti DP, Terrier A. (2016). Identification of elastic properties of human patellae using micro finite element analysis, Journal of Biomechanics, DOI: 10.1016/j.jbiomech.2016.07.031.

[24] Liu, X. S., Cohen, A., Shane, E., Stein, E., Rogers, H., Kokolus, S. L., ... & Guo, X. E. (2010). Individual trabeculae segmentation (ITS)–based morphological analysis of high-resolution peripheral quantitative computed tomography images detects abnormal trabecular plate and rod microarchitecture in premenopausal women with idiopathic osteoporosis. Journal of bone and mineral research, 25(7), 1496-1505.

[25] Lorensen, W. E., & Cline, H. E. (1987, August). Marching cubes: A high resolution 3D surface construction algorithm. In ACM siggraph computer graphics (Vol. 21, No. 4, pp. 163-169). ACM.

[26] MacNeil, J. A., & Boyd, S. K. (2007a). Load distribution and the predictive power of morphological indices in the distal radius and tibia by high resolution peripheral quantitative computed tomography. Bone, 41(1), 129-137.

[27] MacNeil, J. A., & Boyd, S. K. (2007b). Accuracy of high-resolution peripheral quantitative computed tomography for measurement of bone quality. Medical engineering & physics, 29(10), 1096-1105.

[28] MacNeil, J. A., & Boyd, S. K. (2008). Improved reproducibility of high-resolution peripheral quantitative computed tomography for measurement of bone quality. Medical engineering & physics, 30(6), 792-799.

[29] Maquer, G., Musy, S. N., Wandel, J., Gross, T., & Zysset, P. K. (2015). Bone volume fraction and fabric anisotropy are better determinants of trabecular bone stiffness than other morphological variables. Journal of Bone and Mineral Research, 30(6), 1000-1008.

[30] Moreno, R., Borga, M., & Smedby, Ö. (2014). Techniques for computing fabric tensors: a review. In Visualization and Processing of Tensors and Higher Order Descriptors for Multi-Valued Data (pp. 271-292). Springer Berlin Heidelberg.

[31] Moreno, R., Smedby, Ö., & Pahr, D. H. (2015). Prediction of apparent trabecular bone stiffness through fourth-order fabric tensors. Biomechanics and modeling in mechanobiology, 1-14.

[32] Muller, R., Hildebrand, T., & Ruegsegger, P. (1994). Non-invasive bone biopsy: a new method to analyse and display the three-dimensional structure of trabecular bone. Physics in medicine and biology, 39(1), 145.

[33] Müller, R., Hildebrand, T. H. H. J., Häuselmann, H. J., & Rüegsegger, P. (1996). In vivo reproducibility of three-dimensional structural properties of noninvasive bone biopsies using 3D-pQCT. Journal of Bone and Mineral Research, 11(11), 1745-1750.

[34] Müller, R., Van Campenhout, H., Van Damme, B., Van der Perre, G., Dequeker, J., Hildebrand, T., & Rüegsegger, P. (1998). Morphometric analysis of human bone biopsies: a quantitative structural comparison of histological sections and micro-computed tomography. Bone, 23(1), 59-66.

[35] Musy S.N., Maquer G, Panyasantisuk J, Wandel J, Zysset, P. K. (2017) Not only stiffness, but also yield strength of the trabecular structure determined by non-linear μFE is best predicted by bone volume fraction and fabric tensor. J Mech Behav Biomed Mater. 65, 808–813.

[36] Nazemi, S. M., Cooper, D. M., & Johnston, J. D. (2016). Quantifying trabecular bone material anisotropy and orientation using low resolution clinical CT images: A feasibility study. Medical Engineering & Physics. doi:10.1016/j.medengphy.2016.06.011

[37] Nishiyama, K. K., Macdonald, H. M., Hanley, D. A., & Boyd, S. K. (2013). Women with previous fragility fractures can be classified based on bone microarchitecture and finite element analysis measured with HR-pQCT. Osteoporosis International, 24(5), 1733-1740.

[38] Odgaard, A. (1997). Three-dimensional methods for quantification of cancellous bone architecture. Bone, 20(4), 315-328.

[39] Odgaard, A., Kabel, J., van Rietbergen, B., Dalstra, M., & Huiskes, R. (1997). Fabric and elastic principal directions of cancellous bone are closely related. Journal of biomechanics, 30(5), 487-495.

[40] Panyasantisuk, J., Pahr, D. H., & Zysset, P. K. (2015). Effect of boundary conditions on yield properties of human femoral trabecular bone. Biomechanics and modeling in mechanobiology, 1-11.

[41] Pauchard, Y., Liphardt, A. M., Macdonald, H. M., Hanley, D. A., & Boyd, S. K. (2012). Quality control for bone quality parameters affected by subject motion in high-resolution peripheral quantitative computed tomography. Bone, 50(6), 1304-1310.

[42] Rao, A. R., & Schunck, B. G. (1991). Computing oriented texture fields. CVGIP: Graphical Models and Image Processing, 53(2), 157-185.

[43] Richy, F., Ethgen, O., Bruyere, O., Mawet, A., & Reginster, J. Y. (2004). Primary prevention of osteoporosis: mass screening scenario or prescreening with questionnaires? An economic perspective. Journal of Bone and Mineral Research, 19(12), 1955-1960.

[44] Simmons, C. A., & Hipp, J. A. (1997). Method-based differences in the automated analysis of the three-dimensional morphology of trabecular bone. Journal of Bone and Mineral Research, 12(6), 942-947.

[45] Sode, M., Burghardt, A. J., Nissenson, R. A., & Majumdar, S. (2008). Resolution dependence of the non-metric trabecular structure indices. Bone, 42(4), 728-736.

[46] Tabor, Z., and E. Rokita. Quantifying anisotropy of trabecular bone from gray-level images. Bone 40(4):966–972,2007.

[47] Tabor, Z. (2012). Equivalence of mean intercept length and gradient fabric tensors–3d study. Medical engineering & physics, 34(5), 598-604.

Article in Bone · January 2017 - DOI: 10.1016/j.bone.2017.01.016

[48] Varga, P., & Zysset, P. K. (2009a). Sampling sphere orientation distribution: an efficient method to quantify trabecular bone fabric on grayscale images. Medical image analysis, 13(3), 530-541.

[49] Varga, P., & Zysset, P. K. (2009b). Assessment of volume fraction and fabric in the distal radius using HR-pQCT. Bone, 45(5), 909-917.

[50] Varga, P., Dall'Ara, E., Pahr, D. H., Pretterklieber, M., & Zysset, P. K. (2011). Validation of an HR-pQCT-based homogenized finite element approach using mechanical testing of ultra-distal radius sections. Biomechanics and modeling in mechanobiology, 10(4), 431-444.

[51] Whitehouse, W. J. (1974). The quantitative morphology of anisotropic trabecular bone. Journal of microscopy, 101(2), 153-168.

[52] Zhou, B., Wang, J., Yu, Y. E., Zhang, Z., Nawathe, S., Nishiyama, K. K., ... & Guo, X. E. (2016). High-resolution peripheral quantitative computed tomography (HR-pQCT) can assess microstructural and biomechanical properties of both human distal radius and tibia: Ex vivo computational and experimental validations. Bone, 86, 58-67.

[53] Zysset, P.K., Curnier, A., 1995. An alternative model for anisotropic elasticity based on fabric tensors. Mech. Mater. 21, 243–250.

[54] Zysset, P. K. (2003). A review of morphology–elasticity relationships in human trabecular bone: theories and experiments. Journal of biomechanics, 36(10), 1469-1485.

Article in Bone · January 2017 - DOI: 10.1016/j.bone.2017.01.016

Figures

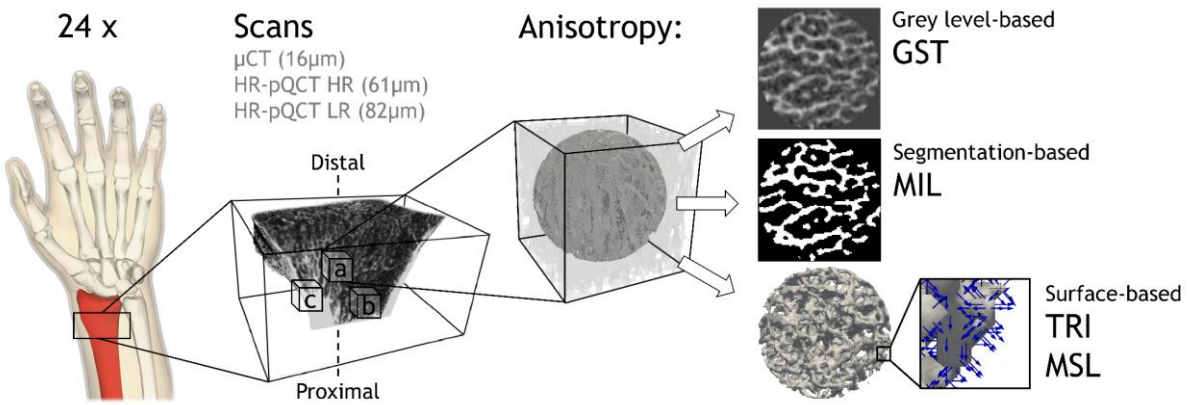

Fig. 1. The distal sections of 24 radii were scanned by µCT100 and HR-pQCT protocols of the XtremeCT II (SCANCO Medical AG, Brüttisellen, Switzerland). A cohort of 182 cubes per modality was generated by cropping cubic regions of interest from the high (a) and low (b) density trabecular core and near the cortex (c). The anisotropy of each cube was measured by the fabric tensors computed from the grey level images via GST, from the segmented images via MIL and from surface meshes via TRI and MSL. TRI and MSL are based on the vectors normal (blue) to the triangle elements of the surface meshes.

Article in Bone · January 2017 - DOI: 10.1016/j.bone.2017.01.016

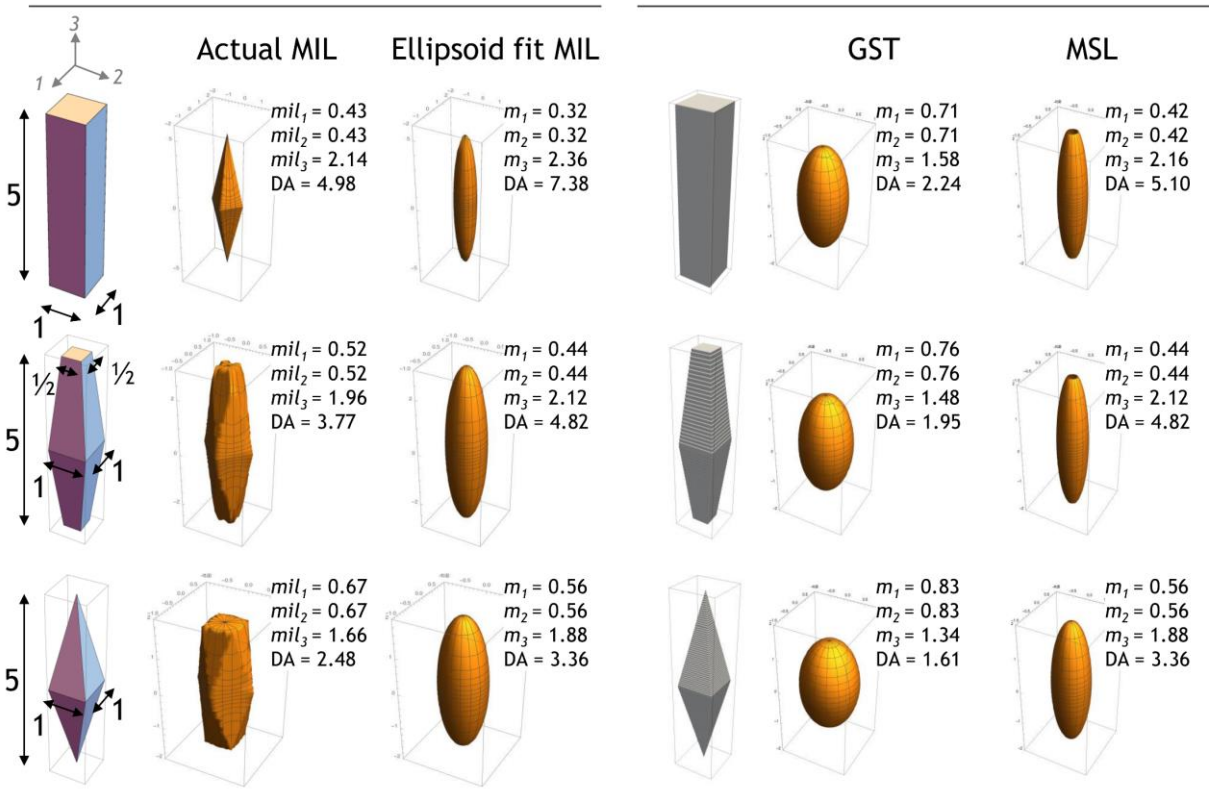

Fig. 2. Eigenvalues (m_i) and degree of anisotropy (DA) of hexahedron, truncated and full octoahedra (from top to bottom). MIL distribution and its ellipsoidal approximation are calculated on the analytical surfaces (left column), GST and MSL fabric tensors are evaluated after voxelization of the surfaces (right column). NB: Unlike the other methods, MSL does not generate an orientation distribution, but directly yields a system of eigenvectors and eigenvalues. The ellipsoid is thus not required for MSL and was merely used as a representation for comparison with the other methods.

Article in Bone · January 2017 - DOI: 10.1016/j.bone.2017.01.016

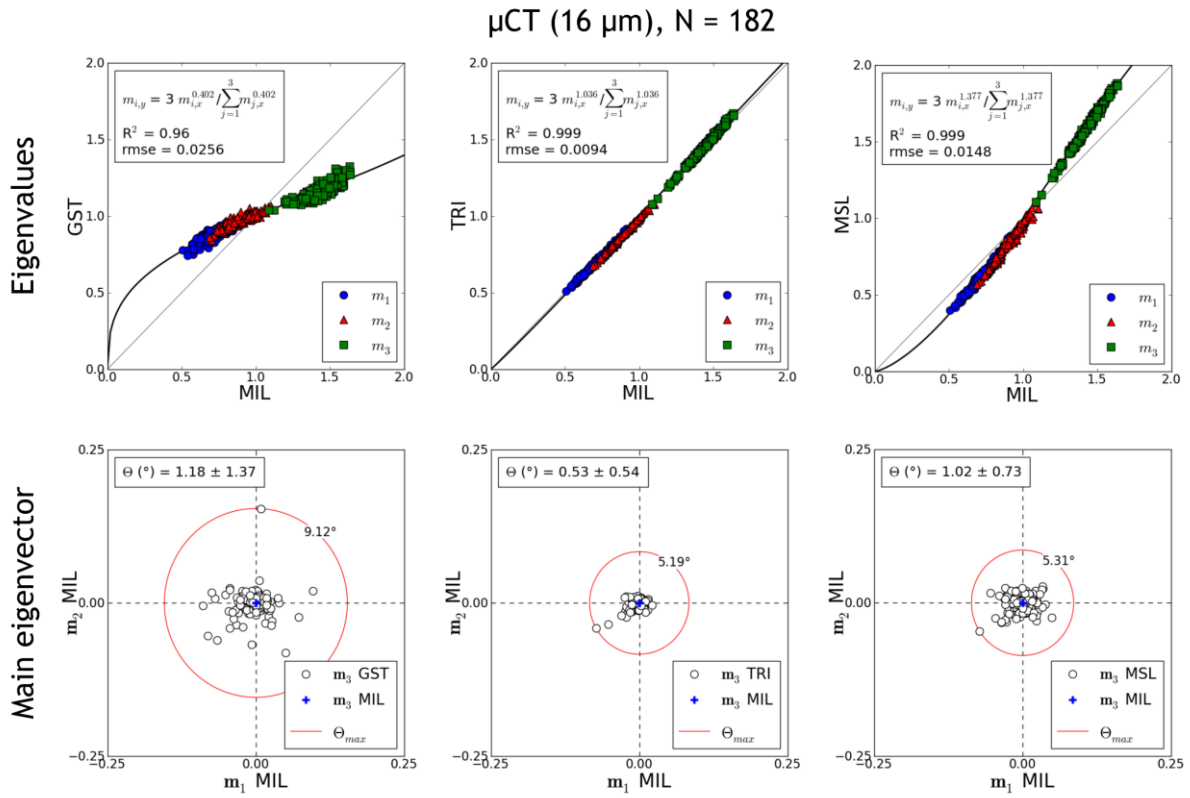

Fig. 3. GST, TRI and MSL fabric tensors evaluated on μCT scans is compared to **MIL$_{\mu CT}$**. The deviation between eigenvalues is quantified by exponent *k*, goodness of fit (R^2) and root-mean-square errors (rmse) of the power relationship (eq, 4). The spread of the tensor's main eigenvector (**m3**) around **MIL$_{\mu CT}$**'s **m3** is displayed in the fabric coordinate system of **MIL$_{\mu CT}$**. The mean, standard deviation, and maximum value of the corresponding angular deviation between main eigenvectors (θ) are also provided.

Article in Bone · January 2017 - DOI: 10.1016/j.bone.2017.01.016

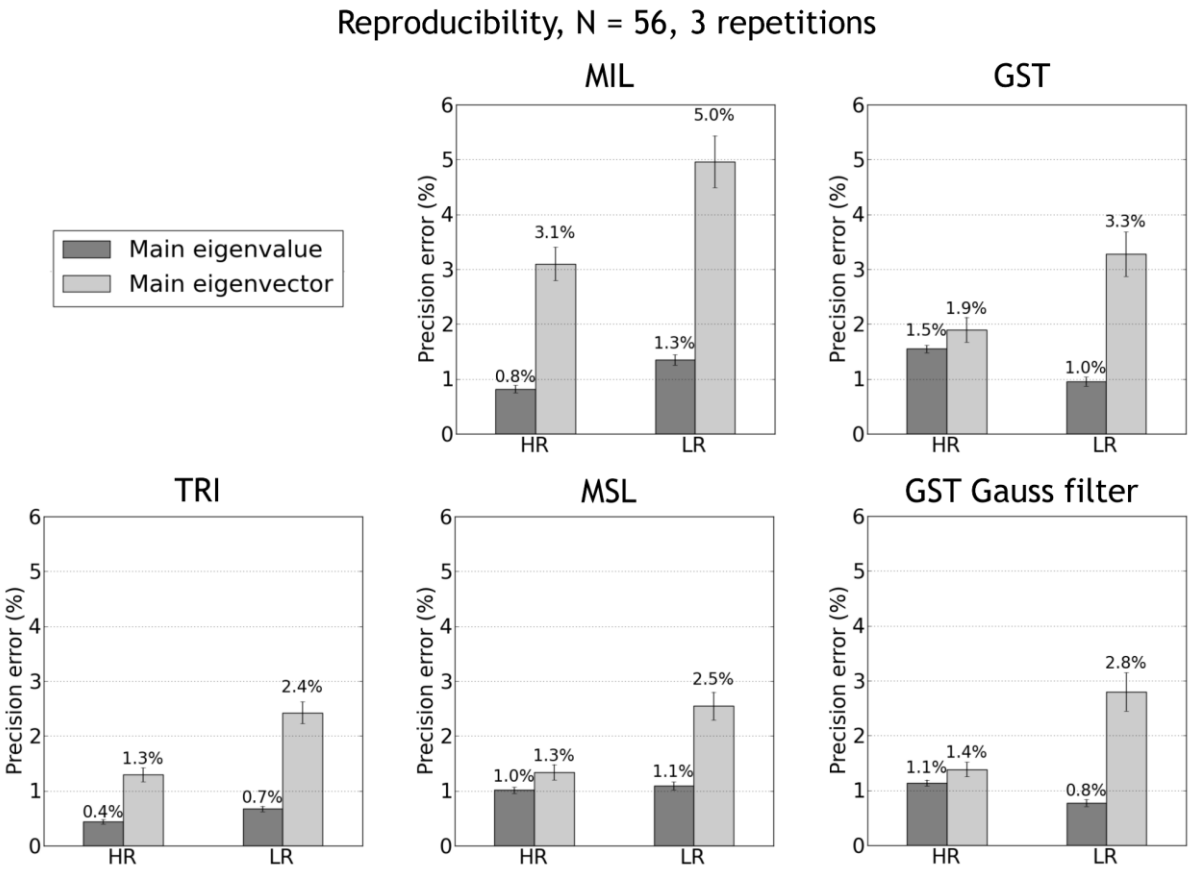

Fig. 4. Reproducibility of the main eigenvalue (m_3) and main eigenvector ($\mathbf{m_3}$) of MIL, GST, TRI and MSL fabric tensors depends on the HR-pQCT protocols (HR: 61µm, LR: 82µm).

Article in Bone · January 2017 - DOI: 10.1016/j.bone.2017.01.016

Tables

	µCT	HR	LR
Bone volume fraction	0.14 ± 0.06 range [0.04; 0.27]	0.21 ± 0.10 range [0.03; 0.43]	0.20 ± 0.08 range [0.04; 0.40]
Degree of anisotropy			
MIL	2.10 ± 0.30 range [1.22; 2.82]	1.86 ± 0.23 range [1.19; 2.53]	1.85 ± 0.23 range [1.15; 2.68]
GST	1.35 ± 0.12 range [1.07; 1.69]	1.41 ± 0.14 range [1.09; 1.78]	1.55 ± 0.16 range [1.13; 2.12]
GST Gauss filter	-	1.50 ± 0.16 range [1.08; 1.98]	1.61 ± 0.18 range [1.14; 2.24]
TRI	2.14 ± 0.32 range [1.20; 2.90]	1.81 ± 0.22 range [1.16; 2.45]	1.76 ± 0.21 range [1.14; 2.43]
MSL	2.76 ± 0.54 range [1.27; 4.12]	2.28 ± 0.38 range [1.22; 3.33]	2.23 ± 0.36 range [1.21; 3.4]

Table 1. The morphology (mean ± standard deviation, range [min; max]) of our samples is given on the three resolutions (µCT: 16µm, HR: 61 µm, LR: 82µm).

Article in Bone · January 2017 - DOI: 10.1016/j.bone.2017.01.016

	MIL		GST			GST Gauss filter		TRI			MSL		
	HR	LR	µCT	HR	LR	HR	LR	**µCT**	HR	LR	µCT	**HR**	**LR**
Eigenvalues													
k	0.81	0.80	0.40	0.47	0.59	0.56	0.64	**1.04**	0.79	0.75	1.38	**1.09**	**1.07**
R^2	0.98	0.98	0.96	0.96	0.97	0.97	0.97	**0.99**	0.99	0.98	0.99	**0.99**	**0.99**
rmse	0.03	0.04	0.03	0.03	0.03	0.03	0.03	**0.01**	0.03	0.03	0.02	**0.04**	**0.04**
Main eigenvector													
θ (°)	2.54±2.73	2.59±2.55	1.18±1.37	2.23±1.98	2.51±2.02	2.0±1.68	2.57±2.21	**0.53±0.54**	2.22±2.28	2.32±2.06	1.02±0.73	**2.03±2.02**	**2.05±1.98**

Table 2. MIL, GST, TRI and MSL fabric tensors evaluated on three resolutions (µCT: 16µm, HR: 61 µm, LR: 82µm) are compared to $\mathbf{MIL_{\mu CT}}$. The deviation between eigenvalues is given by exponent *k*, goodness of fit (R^2) and root-mean-square errors (rmse) of the power relationship (eq, 4). The angular deviation between the main eigenvectors of the current fabric tensor and $\mathbf{MIL_{\mu CT}}$ (θ) is characterised by mean, standard deviation and range [min; max]. The best surrogate of $\mathbf{MIL_{\mu CT}}$ for each image resolution is highlighted by a **bold** font.